

High-entropy alloys in thermoelectric application: A selective review

Kai Ren(任凯), Wenyi Huo(霍文燚), Shuai Chen(陈帅), Yuan Cheng(程渊), Biao Wang(王彪), and Gang Zhang(张刚)

Citation: Chin. Phys. B, 2024, 33 (**5**): 057202. DOI: 10.1088/1674-1056/ad34c5
Journal homepage: http://cpb.iphy.ac.cn; http://iopscience.iop.org/cpb

What follows is a list of articles you may be interested in

Ga intercalation in van der Waals layers for advancing p-type Bi_2Te_3-based thermoelectrics

Yiyuan Chen(陈艺源), Qing Shi(石青), Yan Zhong(钟艳), Ruiheng Li(李瑞恒), Liwei Lin(林黎蔚), Ding Ren(任丁), Bo Liu(刘波), and Ran Ang(昂然)
Chin. Phys. B, 2023, 32 (**6**): 067201. DOI: 10.1088/1674-1056/acc2af

Advancing thermoelectrics by suppressing deep-level defects in Pb-doped $AgCrSe_2$ alloys

Yadong Wang(王亚东), Fujie Zhang(张富界), Xuri Rao(饶旭日), Haoran Feng(冯皓然), Liwei Lin(林黎蔚), Ding Ren(任丁), Bo Liu(刘波), and Ran Ang(昂然)
Chin. Phys. B, 2023, 32 (**4**): 047202. DOI: 10.1088/1674-1056/acb765

Effect of carbon nanotubes addition on thermoelectric properties of $Ca_3Co_4O_9$ ceramics

Ya-Nan Li(李亚男), Ping Wu(吴平), Shi-Ping Zhang(张师平), Yi-Li Pei(裴艺丽), Jin-Guang Yang(杨金光), Sen Chen(陈森), and Li Wang(王立)
Chin. Phys. B, 2022, 31 (**4**): 047203. DOI: 10.1088/1674-1056/ac4bd2

Thermoelectric performance of XI_2 (X = Ge, Sn, Pb) bilayers

Nan Lu(陆楠) and Jie Guan(管杰)
Chin. Phys. B, 2022, 31 (**4**): 047201. DOI: 10.1088/1674-1056/ac474c

Significant role of nanoscale Bi-rich phase in optimizing thermoelectric performance of Mg_3Sb_2

Yang Wang(王杨), Xin Zhang(张忻), Yan-Qin Liu(刘燕琴), Jiu-Xing Zhang(张久兴), Ming Yue(岳明)
Chin. Phys. B, 2020, 29 (**6**): 067201. DOI: 10.1088/1674-1056/ab84cd

---

TOPICAL REVIEW — Heat conduction and its related interdisciplinary areas

High-entropy alloys in thermoelectric application: A selective review

Kai Ren(任凯)[1,†], Wenyi Huo(霍文燚)[2,†], Shuai Chen(陈帅)[3], Yuan Cheng(程渊)[4,5,‡], Biao Wang(王彪)[6,§], and Gang Zhang(张刚)[7,¶]

[1] *Zhengzhou University Advanced Medical Research Center, Luoyang Central Hospital, Luoyang* 471099, *China*
[2] *School of Mechanical and Electronic Engineering, Nanjing Forestry University, Nanjing* 210037, *China*
[3] *Materials Genome Institute, Shanghai University, Shanghai* 200444, *China*
[4] *Monash Suzhou Research Institute, Monash University, Suzhou* 215000, *China*
[5] *Department of Materials Science and Engineering, Monash University, Clayton VIC* 3800, *Australia*
[6] *Research Institute of Interdisciplinary Science, Dongguan University of Technology, Dongguan* 523808, *China*
[7] *Yangtze Delta Region Academy of Beijing Institute of Technology, Jiaxing* 314019, *China*

(Received 12 November 2023; revised manuscript received 4 March 2024; accepted manuscript online 18 March 2024)

Since the superior mechanical, chemical and physical properties of high-entropy alloys (HEAs) were discovered, they have gradually become new emerging candidates for renewable energy applications. This review presents the novel applications of HEAs in thermoelectric energy conversion. Firstly, the basic concepts and structural properties of HEAs are introduced. Then, we discuss a number of promising thermoelectric materials based on HEAs. Finally, the conclusion and outlook are presented. This article presents an advanced understanding of the thermoelectric properties of HEAs, which provides new opportunities for promoting their applications in renewable energy.

Keywords: high-entropy alloys, thermoelectric materials, thermal conduction

PACS: 72.15.Jf, 73.50.Lw, 61.66.Dk **DOI:** 10.1088/1674-1056/ad34c5

1. Introduction

For thousands of years, to improve the performance of metallic materials, the most conventional method is to introduce new alloying elements into the principal element, thus, an alloy family based on the main elements is formed. For instance, steel,[1] aluminum,[2] titanium and nickel[3] alloys are characterized by the principal elements Fe, Al, Ti and Ni, respectively. Nowadays, alloys have widely been used in various applications because of their desirable properties. Magnesium possesses high strength and a decent weight ratio and is a popular material for automotive and aerospace applications.[4,5] The large deformation capacity and micromachinability of shape memory alloys promote the microsystems design.[6] Fashionably, aluminum can be used as an anode electrode, which has a capacity of up to 110 mAh/g combined with graphite.[7] Besides, alloys at the nanoscale exhibit more interesting ductility, mechanical strength and thermoelectric properties, as reported by experimental and theoretical investigations.[8–13] Although these factors effectively improve the properties of alloys, alloys with a certain element as the main body greatly limit the type of alloy combination and the new generation development of alloy materials.[14] Therefore, advanced strategies are essential to expand the types and applications of alloys.

Recently, the approach to compound multiple principal elements together as a high concentration steady state has become quite popular,[15,16] named high-entropy alloys (HEAs), which can overcome the restriction of conventional alloy development and were first proposed by Cantor and Yeh *et al.* in 2004.[17,18] Although HEAs are formed by multiple components, they still possess unique microstructural stability.[19,20] For mechanical properties, the HEAs reveal a wide range of yield strengths, such as 300 MPa ($AlCoCrFeNiTi_x$)[21] and $\sim 10^3$ MPa (NbMoTaW),[22] which can even be tuned by varying the concentrations of constituent elements.[23–25] Interestingly, HEAs still preserve such novel mechanical properties at elevated (e.g., $Al_xCrFeCoNi$, CrMnFeCoNi,[26] FeCoNiCrMn[27] and $Nb_{25}Ta_{25}Mo_{25}W_{25}$[26]) and cryogenic temperatures (e.g., $Al_{0.6}CoCrFeNi$,[28] $Al_{0.3}CoCrFeNi$,[29] and TiZrHfNbTa[30]). HEAs also suggest excited fatigue[31] and wear[32] characteristics and all those mechanical properties are phase structure dependent.[33–35] HEAs even show promising physical performance, such as magnetic ordering, which is commonly derived from specific elements (Cu, Ti, Al, Co, Fe, etc.).[36] Some flexible magnetic properties have been reported in $AlCo_xCr_{1-x}FeNi$,[37] FeCoCrNiAlCu,[38] and $Al_xCoCrFeNi$,[39] suggesting soft and hard magnetic component applications.[40] In particular, some HEAs reveal noble biocompatible and chemical performances as biomedical

[†]These authors contributed equally to this work.
[‡]Corresponding author. E-mail: yuan.cheng@monash.edu
[§]Corresponding author. E-mail: wangbiao@mail.sysu.edu.cn
[¶]Corresponding author. E-mail: gangzhang2006@gmail.com

© 2024 Chinese Physical Society and IOP Publishing Ltd

devices (TiZrNbHfTa and TiZrNbHfTa coatings)[41] and supercapacitor electrodes (AlCoCrFeNi).[42] These demonstrate the unique advantages of HEAs compared with traditional alloys.[43]

In recent decades, the ever-growing energy demand has become one of the world's biggest challenges.[44] Moreover, the usage of fossil fuels also brings critical environmental problems.[45] To solve energy and environmental issues, the development of a clean energy system is essential.[46] Tremendous investigations have focused on using HEAs as an electrode to decompose water in the hydrogen evolution reaction (HER) and oxygen evolution reaction (OER),[47–50] but ignored HEAs are also promising candidates in thermoelectric applications. Thermoelectric devices can directly convert waste heat into electricity, thus, they are an effective way to solve the global energy crisis.[51] In principle, the strong phonon scattering progress in HEAs can be exhibited simultaneously because of the increased complexity of the materials. Because the atoms have different atomic sizes and electronegativities, the enthalpy change is a combination in the internal strain energy due to atomic size mismatch and fluctuations of the internal ionic field energy arising from electron cloud redistribution.[52] Interestingly, traditional alloy using as thermoelectrics has significant investigations. The thermoelectric properties of PbTe–SrTe system can be improved by the Na-doped method.[53] The $Bi_{0.52}Sb_{1.48}Te_3$ is prepared by a melt spinning (MS) technique with 5 nm–15 nm fine nanocrystalline, which also presents an excellent figure of merit ZT value of 1.56 at 300 K.[54] $Fe_2V_{0.8}W_{0.2}Al$ is synthesized using magnetron sputtering method, suggesting a high intrinsic figure of merit characteristic.[55] Thus, HEAs used as thermoelectric devices are worth looking forward to.

In this review, we present the state-of-the-art advances in the thermoelectric properties of HEAs, focusing on the physical insights into reduced lattice thermal conductivity and enhanced Seebeck coefficient. The rest of this article is organized as follows. In Section 2, we first provide a brief review on the basic concepts and characteristics of HEAs, such as the definition, crystalline, quasicrystalline and amorphous structural characteristics. Then, in Section 3, we discuss the recent advances in the thermoelectric properties of HEAs. The intrinsic advantages of HEAs in thermoelectric applications are addressed by the phonon properties in group-IV metal chalcogenides and Bi_2Te_3. Finally, we give a brief conclusion and outlook for future experimental and theoretical studies in Section 4.

2. Basic insights of HEAs

2.1. Definition of HEAs

In the two influential papers published in 2004,[56,57] a novel strategy was suggested to obtain HEAs via developing the unknown center of multicomponent phase diagrams. Initially, the promising group of alloys was defined as solid solution alloys that contain more than five elements with equal (or near) atomic percent (at.%),[58] and the atomic fraction of each component was greater than 5 at.%. The multicomponent alloys are well away from the edges and corners of the phase diagrams. The birth of the unusual concept overturns human-beings' inherent ideas for designing and making materials.

The mixing entropy of materials ($\Delta S^0_{\rm mix}$) can be determined by[57]

$$\Delta S^0_{\rm mix} = \Delta S^0_{\rm conf} + \Delta S^0_{\rm vib} + \Delta S^0_{\rm mag} + \Delta S^0_{\rm elec}, \tag{1}$$

where $\Delta S^0_{\rm conf}$, $\Delta S^0_{\rm vib}$, $\Delta S^0_{\rm mag}$, and $\Delta S^0_{\rm elec}$ are the configurational entropy, vibrational entropy, magnetic dipole entropy, and electronic randomness entropy, respectively. In particular, $\Delta S^0_{\rm conf}$ occupies a very important position where an alloy composed of elements with equal atomic ratios can be calculated by Boltzmann's assumption,[59]

$$\begin{aligned}\Delta S_{\rm conf} &= -R\left(\frac{1}{n}\ln\frac{1}{n}+\frac{1}{n}\ln\frac{1}{n}+\cdots\frac{1}{n}\ln\frac{1}{n}\right)\\ &= -R\ln\frac{1}{n} = R\ln n,\end{aligned} \tag{2}$$

where R is the gas constant, about 8.3145 J·mol^{-1}·K^{-1}), and n is the number of constituent elements. The configurational entropy of alloys with different component numbers is shown in Fig. 1.

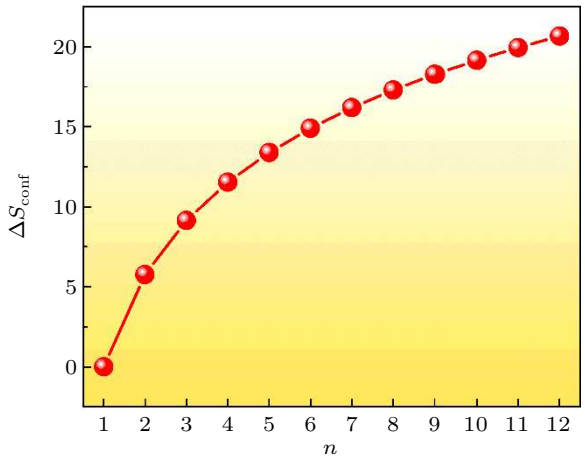


Fig. 1. The relationship between mixed entropy and number of elements.

It is worth noting that, when $n = 1$, a single element constitutes a pure metal, suggesting that its configurational entropy is zero. When $n = 2$, its configurational entropy is $0.69R$. When $n = 3$, 4 and 5, it is rapidly increased to $1.10R$, $1.39R$, and $1.61R$, respectively. When $n = 15$, the configurational entropy reaches $2.71R$. The overall rule is that as the number of principal components n increases, the mixing entropy continues to increase, and the increase in its magnitude slows down as the number of components increases. An alloy composed of 5 or more elements with $S \geq 1.5R$ can be

referred to as an HEA.[60] In addition, the quaternary alloy with $S \geq 1.36R$ is also able to qualify as the HEAs. Thus, the configurational entropy ($1.5R$) can be used as the standard to distinguish high/medium entropy alloys.

Figure 2(a) presents the schematic ternary and quaternary phase diagrams showing regions of well-known materials near the corners and edges and regions of less studied or unknown materials in the center.[61] Taking body-centered cubic (BCC) as an example, it shows the schematics of lattice distortion in pure metals, conventional dilute alloys, and high-entropy alloys in Fig. 2(b).[62] An illustration of the $\Delta S^0_{\rm mix}$ for the ternary alloy system is shown in Fig. 2(c).[63] Based on 13 principal elements, through permutation and combination, 7099 chemical compositions of HEAs with atomic ratios ranging from five to thirteen elements are designed.[57] It is $C_5^{13}+C_6^{13}+C_7^{13}+C_8^{13}+C_9^{13}+C_{10}^{13}+C_{11}^{13}+C_{13}^{13}=7099$. In view of the potential for microalloying, the number of HEAs that can be designed and explored will be even more amazing. In Fig. 2(d), it shows the common elements included in the HEAs and the classification of various HEAs. In theory, it is suspected that a high configurational entropy can stabilize and optimize a random solid solution to form HEAs,[62] so the concept of HEAs is expanded. Quaternary alloys that comply with the high-entropy strategy are named as HEAs.[64–66]

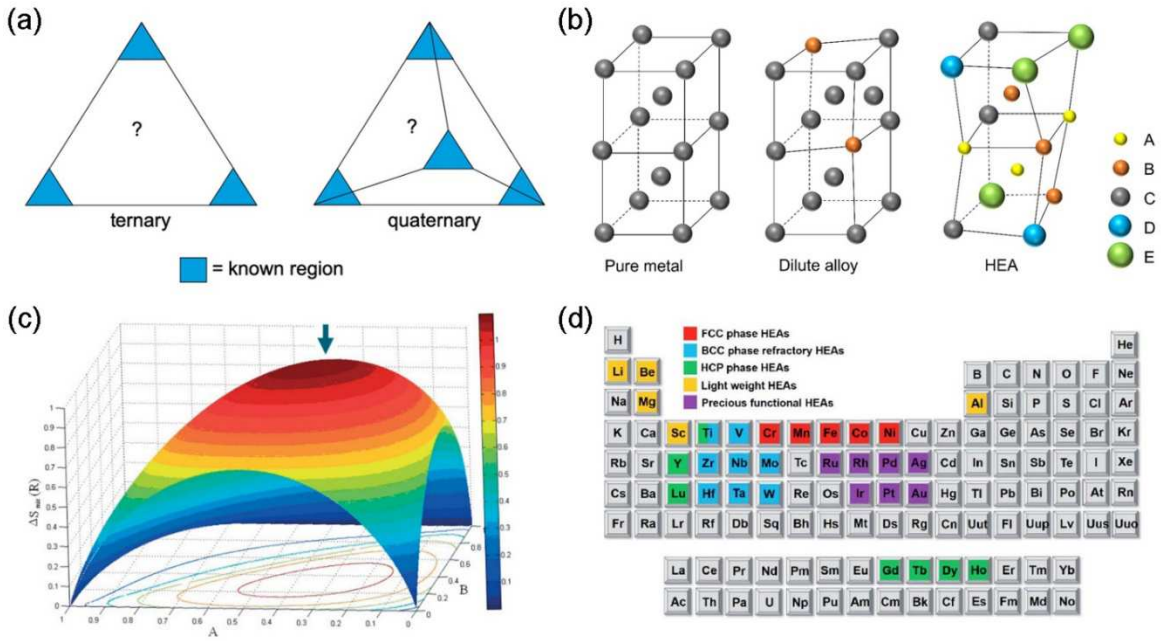


Fig. 2. (a) Schematic ternary and quaternary phase diagrams showing regions of well-known materials near the corners and edges and regions of less-known or unknown materials in the center.[61] For more details, please refer to Ref. [61]. (b) Schematics of lattice distortion in body-centered cubic pure metals, conventional dilute alloys, and high-entropy alloys. A–E represent different element species in general.[62] For more details, please refer to Ref. [62]. (c) Illustration of the $\Delta S^0_{\rm mix}$ for ternary alloy system.[63] For more details, please refer to Ref. [63]. (d) Common elements included in the HEAs and classification of various HEAs.[67] For more details, please refer to Ref. [67].

The four core effects of HEAs are high-entropy effect, sluggish diffusion effect, severe lattice distortion effect, and cocktail effect.[58] In 2004, Yeh[57] firstly reported that, high entropy is the unique effect of HEAs since it enhances the formation of single solution phases, and as a result, it makes the microstructure much simpler than previously expected. Overall, a higher number of elements allow the random state to have the mixing enthalpy closer to that of the completely ordered state.[57] Thus, it becomes even more competitive with the ordered state under the aid of its high mixing entropy. In detail, it shows that the increased configurational entropy could facilitate the formation of solid solution phases by lowering the corresponding free energy, especially at higher temperatures. Although it is suspected that a high configurational entropy stabilizes and optimizes a random solid solution to form HEAs, there is a fact that most HEAs show simple structure.[61]

The sluggish diffusion effect means that in HEAs, the diffusion process is relatively slow, which is beneficial to the preparation of some specific microstructures. The diffusion coefficient of the elements in HEAs is compared with those of the elements in pure metals and stainless steels and it is found that the HEAs have the slowest diffusion coefficient, because the diffusion and phase transformation kinetics are slow in HEAs.[68,69] During diffusion, the neighboring atoms in HEAs are somewhat different when an atom jumps into the vacancy, due to the random distribution of atoms. The atom becomes trapped and difficult to deviate from the site when it jumps into a low-energy site. The case would be the opposite when it is a high-energy site. Under both cases, the diffusion process is hindered.[70] This effect could be used to explain the formation of nano-sized precipitates, because nuclei easily form but grow slowly.[57] In the as-cast CuCoNiCrFe

HEA, nano-precipitates with a size of 7 nm–50 nm in diameter, close to the face-centered cubic phase in a spinodal plate, appear, as shown in Figs. 3(a)–3(e).[57] On the other hand, it demonstrates the promising potential of HEAs for application in diffusion barrier coatings.

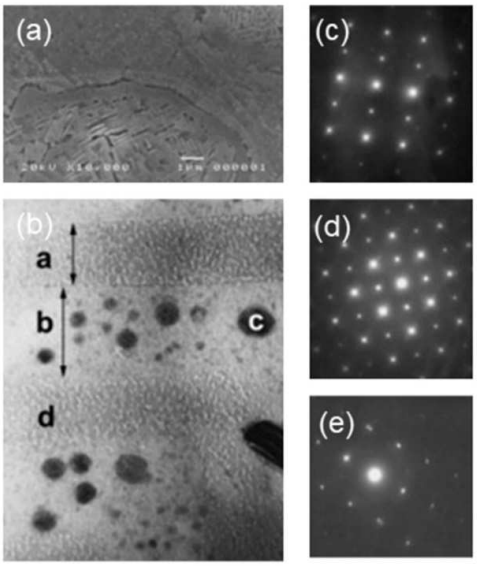


Fig. 3. Microstructures of an as-cast CuCoNiCrAlFe alloy. (a) SEM micrograph. (b) TEM bright-field image. (c)–(e) Corresponding selected area diffraction (SAD) patterns of (b) with zone axes of BCC [0 1 1], BCC [0 0 1] + (0 1 0) superlattice, and FCC [0 1 1], respectively.[57] For more details, please refer to Ref. [57].

The severe lattice distortion effect of HEAs is usually compared with the alloys with a certain dominant element. In HEAs, the lattice site is occupied by random atoms. The neighboring atoms usually have different atomic sizes, bond configurations, and lattice potential energies. There are several impacts on the mechanical properties of HEAs from the severe lattice distortion effect.[71] For instance, enhanced hardness and strength can be obtained from HEAs.[72]

The cocktail effect was first proposed by Ranganathan,[73] aiming to describe the process of synergistic mixing of the elements in HEAs. It demonstrates that the excellent properties of HEAs are not only derived from the basic properties of the elements under the mixing rule, but also from the interaction between the elements.[74] For example, remarkable antioxidant activity can be obtained in HEAs via introducing a certain element with strong oxidative resistance.[75]

2.2. Structure of HEAs

2.2.1. Crystalline HEAs

The crystalline HEAs can be divided into solid solutions, intermetallic phases, or a mixture of both solid solutions and intermetallic phases. There are three kinds of solid solutions found in HEAs, face centered cubic (FCC), BCC and hexagonal close packed structure.

FCC HEAs are mainly composed of the 3d transition metal elements with equal- (or near-) atomic compositions. Most FCC HEAs show remarkable ductility and considerable strength. Among them, CoCrFeMnNi and CoCrFeNi HEAs are two typical FCC HEAs. They show remarkable mechanical properties even at the temperatures of liquid nitrogen.[76] The elements for BCC HEAs are mainly refractory metal elements. It shows superior thermostability and elevated mechanical properties in BCC HEAs. For example, TaNbMoW and TaNbVMoW HEAs show remarkable mechanical properties at elevated temperatures.[64] They are named as refractory HEAs.[64] It shows the potential of HEAs for high-temperature applications. The representative HCP HEAs include DyGdLuTbY and DyGdLuTbTm,[77] it is found that the rare earth elements prefer to create an HCP structure, due to their similar atomic sizes in favor of the formation of an isomorphic binary solid solution. On the other hand, HCP HEAs can also be obtained via FCC–HCP transformation from their FCC structure,[78] such as the case in $Al_{0.6}$CoCrFeNi HEAs.

On the other hand, for intermetallic compounds, there are topologically close-packed phases (TCPs), e.g., σ, μ, χ, and Laves phases.[79] Recently, several studies show the mixed-phase structures (biphase and even more phases) in HEAs.[80,81] The added phases can be controllably introduced via adjustment of the element concentration.

2.2.2. Amorphous HEAs

Amorphous HEAs are a new type of HEAs, which inherit the advantages of HEAs and amorphous structures. For the sake of obtaining high glass forming ability, at least one kind of metalloid element, e.g., B, C, P, and Si, is usually added to HEAs. There are also several amorphous HEAs without metalloid elements reported.[82] Benefiting from both the amorphous structure and high-entropy effect, amorphous HEAs show specific properties such as high strength, superior wear and corrosion resistance.[83] However, the metastability of amorphous HEAs is a unique characteristic. It makes the amorphous structure in HEAs tends to turn into a crystalline structure when changing the temperature. Amorphous HEAs show various applications in industry, due to their unique physical and chemical properties.[84] Amorphous HEAs can be fabricated with a low critical cooling rate even down to 10 $K{\cdot}s^{-1}$. On the other hand, amorphization can be observed in FCC HEAs subjected to high-pressure torsion.[85]

2.2.3. Quasicrystalline HEAs

Most quasicrystalline structures are dominated by only one element, while those with multiple elements have rarely been discovered. The typical quasicrystalline HEAs with multiple elements are MgMnAlZnCu[86] and $Al_{20}Si_{20}Mn_{20}Fe_{20}Ga_{20}$[87] alloys. In MgMnAlZnCu alloy, the matrix is HCP phase.[86] There are many pits on the matrix, which might be the sites of deciduous quasi-crystal particles.

The retained quasicrystalline phase can be found in a few pits.[86] On the other hand, it reports a decagonal quasicrystalline HEAs, $Al_{20}Si_{20}Mn_{20}Fe_{20}Ga_{20}$.[87] The periodicity is 1.23 nm. The most basic structural tiles of the quasicrystalline HEAs are polygons with an edge length of 0.62 nm such as squashed hexagon, star, boat, bowtie, and decagon.[87] Quasicrystalline HEAs are interesting topics because of both structural and compositional complexity. Amorphous HEAs and quasicrystalline HEAs possess lower thermal conductivity, which suggests promising application for thermoelectric applications.

3. Thermoelectric properties

3.1. Intrinsic advantages of HEAs in thermoelectric applications

Thermoelectric (TE) technology is a particularly attractive option to provide a green and effective way for solving the global energy crisis through direct heat to electricity energy conversion. The energy conversion efficiency of thermoelectric devices depends on the thermoelectric figure of merit (ZT), which is defined as[88]

$$ZT = \frac{S^2\sigma T}{\kappa_{\rm p} + \kappa_{\rm e}}, \tag{3}$$

where S, σ, T, $\kappa_{\rm p}$ and $\kappa_{\rm e}$ are the Seebeck coefficient, electrical conductivity, temperature, phonon thermal conductivity and electron thermal conductivity, respectively. Previously, the following strategies were usually adopted to reduce the lattice thermal conductivity and consequently enhance ZT, including nanostructuring,[89] introducing phonon-vacancy scattering,[90] phonon scattering by point defects,[91] the rattling effect[92] or other phonon scattering processes in the material, which are summarized as phonon engineering.[93] For promoting the thermoelectric performance, low thermal conductivity is preferred, while maintaining a high carrier mobility and Seebeck coefficient. The aforementioned strategies have a significant impact on the lattice thermal conductivity, but a slight influence on the Seebeck coefficient, and even result in suppressed electrical conductivity. While recently some investigations have been explored on the application of high-entropy stable strategies for the synergistic regulation of the electrical and thermal transport properties of materials. The phase composition can be tuned and the performance also can be enhanced by manipulating the configurational entropy of a material using introducing different atomic species. For example, the ZT of n-type PbSe based high-entropy material is improved by 1.8 at 900 K,[94] which is resulted by largely distorted lattices. Thus, the strong phonon scattering is induced and the largely lower lattice thermal conductivity is obtained. Besides, based on ultra-low lattice thermal conductivity obtained by high entropy stabilization, the electrical properties of HEAs also can be improved by modulating the degree of electron localization, which can avoid the effect of disorder introduction on electron transport. The ZT of germanium telluride-based high-entropy materials can be enhanced as 2.7 at 750 K by tuning electron and phonon localization.[95]

The mass fluctuation can lead to significant phonon scattering and broadening, as well as the enhanced phonon scattering strength due to the strain field is induced by the change in atomic size.[44] Moreover, in HEAs, the locally distinct chemical environment results in force constant variations. These force constant variations also lead to additional phonon scattering.[96] Therefore, the large compositional space inherent to HEAs promotes the phonon scattering rate, consequently suppressing the lattice thermal conductivity. More interestingly, the lattice thermal conductivity may be finely tuned by adjusting the relative fractions of each constituent element.

Liu *et al.* reviewed the thermal conductivity of typical TE materials, and found an obvious configuration entropy dependence.[97] As shown in Fig. 4, when the configuration entropy increases, a large decrease in the lattice thermal conductivity is observed. This is a general phenomenon that appears in various thermoelectric materials, including half-Heusler alloys,[98] skutterudites[99] and chalcopyrites.[100] Increasing entropy can result in a greater number of microscopic configurations associated with more lattice defects, thus introducing extra phonon scattering by point defects and grain boundaries.

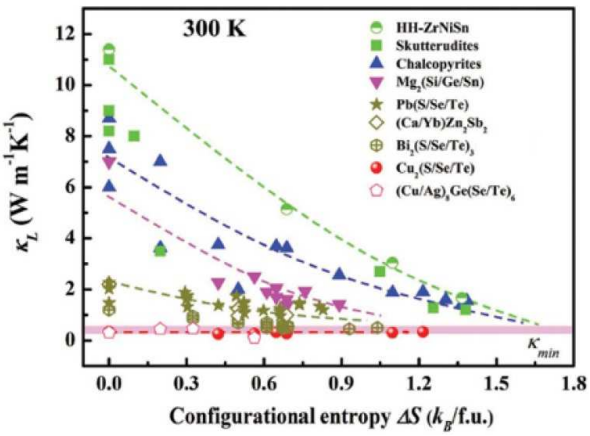


Fig. 4. Lattice thermal conductivity as a function of the configurational entropy.[97] For more details, please refer to Ref. [97].

HEAs also offer the possibility to enhance the Seebeck coefficient and electrical conductivity. As shown in Fig. 5,[97] the Seebeck coefficient increases with configuration entropy. This is induced by the increased crystal symmetry of the material. When the configuration entropy is high, alloys tend to possess a high symmetry structure. For example, single Cu_2Se has a symmetry group of $C2/c$. With the configuration entropy increasing to above 0.6 $k_{\rm B}$/f.u in $Cu_2S_{0.5}Se_{0.5}$, the symme-

try increases to hexagonal. HEAs possess mostly high symmetry crystal structures, including simple face centered cubic (FCC), body centered cubic (BCC), or hexagonal cubic packing (HCP). Therefore, a high Seebeck coefficient in principle can be achieved at an optimal carrier concentration because of the enhanced electronic density-of-states and effective mass induced by the multiple electronic bands around the Fermi level.[101,102] These intrinsic characteristics of HEAs are well aligned with the requirements for good thermoelectric materials.

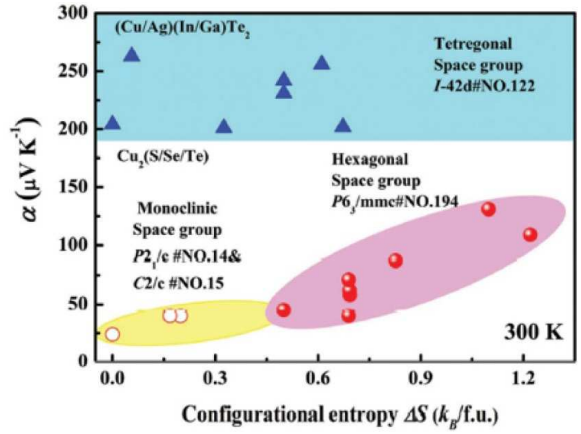


Fig. 5. Seebeck coefficient α as a function of the configurational entropy.[97] For more details, please refer to Ref. [97].

In HEAs, the large mass and force constant fluctuations can induce significant phonon scattering rates. Furthermore, pronounced broadening was observed in the phonon spectrum, which demonstrates the enhanced phonon anharmonicity. Körmann *et al.* employed *ab initio* calculations to explore the phonon spectral broadening of body-centered cubic alloys and studied the dependence on the number of components by changing the alloys from binaries up to 5-component HEAs.[103] Two sets of alloys are studied, set-1 is based on MoTa, including MoTa, MoTaNb, MoTaNbW, and MoTaNbWV, and set-2 is based on VW, including VW, VWNb, VWNbTa, and VWNbTaTi. Figures 6(a)–6(d) show the computed phonon spectra for set-1 and set-2, as demonstrated in Figs. 6(g)–6(j). Figures 6(e) and 6(f) are 3D representations of the long-wavelength spectra for MoTaNbW and MoTaNbWV, respectively. For all considered alloys, the long wavelength phonons are almost unaffected. For phonons in the mid- and high-frequency regions (above ~ 4 THz), the broadening is very strong for both sets of alloys, even up to a few THz. In set-1 of alloys, the broadening of the phonon spectra of 4- and 5-component alloys is much larger than that in the 2- and 3-component alloys at the H-point. This broadening is related to the mass difference and the interaction with chemical disorder. In principle, the lower the atomic mass, the higher the phonon frequency. For example, Mo has a mass of 96 u, and phonon modes mainly contributed from Mo are in the range of 6 THz to 7 THz. On the other side, as Ta has a heavy mass of 181 u, phonon modes mainly contributed from Ta are in the region of about 4 THz to 5 THz. Therefore, with the added element for each alloy, broadening appears in the phonon spectra due to the overlap of some of the newly added phonon peaks. In addition to the mass effect, the force fluctuation in alloys also leads to phonon spectra broadening. In set-2 of alloys, the alloy effect on the phonon spectrum is more obvious. There is a phonon band gap around the H-point (grey dashed lines) in the phonon spectrum of VW. When more elements are added, this band gap disappears because of the overlap of newly added phonon modes.

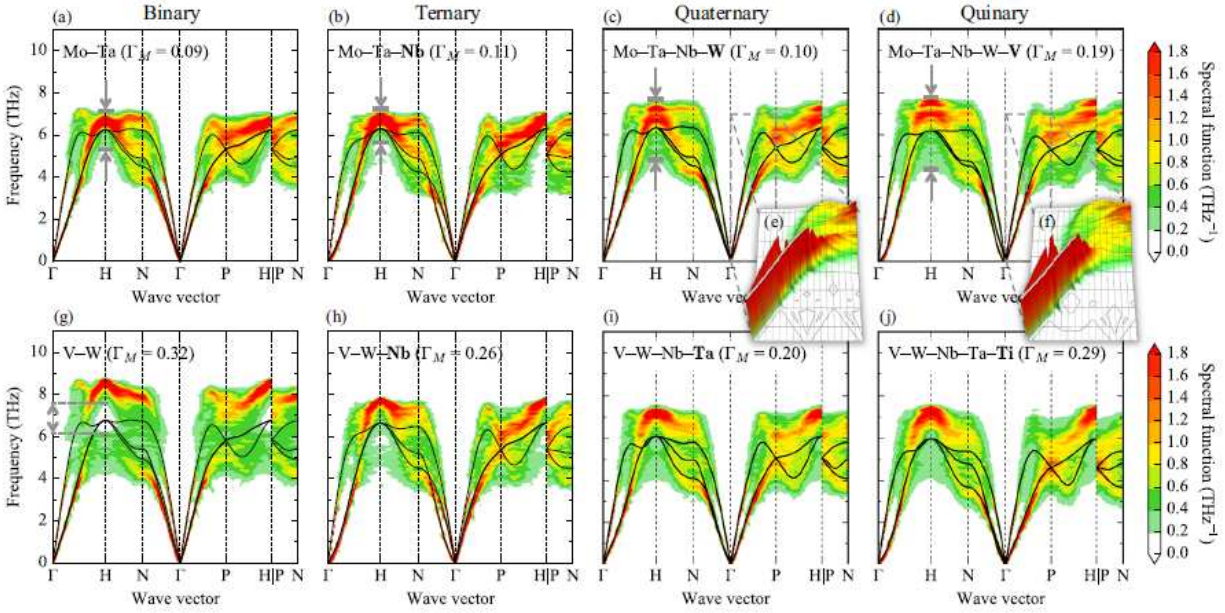


Fig. 6. Broadening of phonon spectra in MoTaNbWV related alloys in panels (a)–(d) and VWNbTaTi related alloys in panels (g)–(j) with increasing number of elements. Γ_{M} is the mass-fluctuation scattering parameter. Panels (e) and (f) are 3D representations of the long-wavelength phonon spectra for MoTaNbW and MoTaNbWV, respectively.[103] For more details, please refer to Ref. [103].

For thermoelectric energy harvesting applications, a high working temperature is an ideal case, because of the large-scale industrial waste heat recovery and high efficiency. In recent years, research attention has been directed towards high temperature thermoelectric materials, including oxides, magnesium silicides, and Zintl compounds.[104] Previously, the state-of-the-art n-type SiGe compounds are promising high temperature thermoelectric materials with $ZT \sim 1$ at $T \geq 800$ °C. In 2015, Shafeie *et al.* synthesized $Al_xCoCrFeNi$ HEAs with high ZT values.[105] At 700 °C, when $x = 0$, the power factor value is close to zero. For $x = 2$, power factor is improved to > 0.2 mW·m^{-1}·K^{-2}, indicating remarkable advantage of HEAs for high temperature thermoelectric application. From the temperature dependent curve, power factor arrives to the maximum value at around 700 °C, then decreases as the temperature increases. From the measured lattice thermal conductivity and power factor at 505 °C, a ZT value of 0.015 is achieved. As the lattice thermal conductivity decreases with increasing temperature in the temperature range of 500 °C–700 °C while the power factor increases, a high ZT is expected at 700 °C. This can open the door towards new thermoelectric materials in high temperature application.

The thermoelectric properties of half-Heusler type $Ti_2NiCoSn_{1-x}Sb_{1+x}$ $(0 < x < 1)$ are explored. It is found for $x = 0$ samples, the microcrystalline samples have a similar thermal conductivity to the bulk TiNiSn sample, and a ZT of 0.144 at 860 K.[106] The value of ZT depends on the content of Sn and Sb, for samples with $x = 0.5$, a ZT of 0.29 at 873 K was reported.[107]

So far, the representative high performance thermoelectric materials include Bi_2Te_3, PbTe, SnSe and SnTe.[108] A direct way to develop thermoelectric HEAs is based on applying known thermoelectric compounds as the starting system. In the following sections, we focus on Bi_2Te_3 based HEAs and IV–VII based HEAs to demonstrate the enhanced thermoelectric in HEAs.

3.2. Bi_2Te_3 based HEAs

Bi_2Te_3 (bismuth telluride) based analogs are the most studied thermoelectric materials with performance peaking near room temperature. In the last decade, some strategies have been suggested to significantly reduce the lattice thermal conductivity and thus enhance ZT, such as nanostructuring,[109] hierarchical structures,[110] and strain engineering.[111] Bi_2Te_3 was successfully applied as the starting material to develop thermoelectric HEAs. In 2016, Fan *et al.*[112] introduced the concept of HEAs to reduce the lattice thermal conductivity of Bi_2Te_3 and markably increased thermoelectric properties were found experimentally in the $BiSbTe_{1.5}Se_{1.5}$ HEA. At 400 K, the lattice thermal conductivity is only 0.47 W·m^{-1}·K^{-1}. In addition, with a small amount of Ag, the lattice thermal conductivity can be further reduced, associated with an increase in the Seebeck coefficient. As shown in Fig. 7, the peak value of the base $BiSbTe_{1.5}Se_{1.5}$ alloy is 0.20 at 450 K. With further alloying with Ag, in the studied temperature range, ZT value increases with Ag alloying, because the Seebeck coefficient increases and the lattice thermal conductivity decreases with Ag content. The maximum ZT value of 0.63 is obtained at 450 K in the 0.9Ag sample, which is about three times than that of the base sample. It is clear that high mixing entropy is effective in enhancing the ZT value. However, when the Ag content is 1.2, the thermoelectric ZT value decreases due to the presence of the Ag-rich secondary phase, which reveals the complexity and challenge in improving the thermoelectric performance of HEAs.

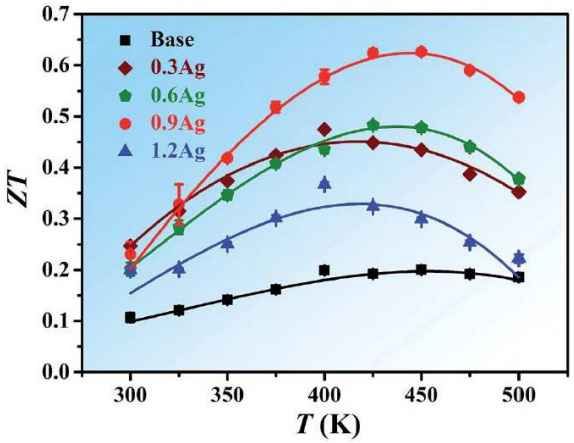


Fig. 7. The thermoelectric figure of merit of $BiSbTe_{1.5}Se_{1.5}Ag_x$ alloys with different x.[112] For more details, please refer to Ref. [112].

The texturing under uniaxial pressure is one of the key factors affecting the thermoelectric properties of Bi_2Te_3-based alloys.[113] The texturing of $BiSbTe_{1.5}Se_{1.5}$ alloy was studied, with the samples synthesized in experiments by self-propagating high-temperature synthesis and spark plasma sintering.[114] Under texturing, a partial ordering of grains was observed, which resulted in the formation of a lamellar grain structure. The orientations of the sheets in adjacent blocks are different from each other. Due to the block texturing, there is an obvious orientation dependence in the thermoelectric properties of the $BiSbTe_{1.5}Se_{1.5}$ alloy. The highest ZT values are 0.43 (perpendicularly to the texturing axis) and 0.34 (parallel to the texturing axis) at 450 K.

A Bi–Te involved HEA, (Ag,Pb,Bi)(S,Se,Te) was synthesized by the congruent melt of Ag powders and grains of Pb, Bi, Te, Se and S at 800 °C, and the thermoelectric properties were investigated.[115] In these HEAs, both cation and anion sites were alloyed and the total entropy reached 2.00R (R is the gas constant). This HEA, $Ag_{0.25}Pb_{0.50}Bi_{0.25}S_{0.40}Se_{0.50}Te_{0.10}$ is an n-type semiconductor with room temperature lattice thermal conductivity of 0.62 W·m^{-1}·K^{-1} and it is further reduced to 0.46 W·m^{-1}·K^{-1} at 723 K. At 723 K, its thermoelectric ZT is ~ 0.54. It is worth noting that although ultralow thermal conductivity is achieved in Bi_2Te_3 based HEAs, this value

of *ZT* is obviously lower than that of state-of-the-art Bi_2Te_3 based analogs because of the reduced electrical conductivity in HEAs. Therefore, in studying high performance thermoelectric HEAs, enhancing the electrical conductivity will be the future focus.

3.3. HEAs based on group-IV metal chalcogenides

Group-IV metal chalcogenides (MCh) such as lead chalcogenides (PbTe, SnSe, PbSe, PbS) have been extensively studied as high efficiency thermoelectric systems.[116,117] Fan *et al.* demonstrated the impact of the HEA concept in promoting thermoelectric performance in PbSnTeSe alloys.[118] At 650 K, the peak value of *ZT* is up to 0.4. The *ZT* value can be further enhanced with La doping, forming $Pb_{1-x}SnTeSeLa_x$ alloys with x in the range of 0–0.1. The minor compositional change not only improve both the Seebeck coefficient and electrical conductivity, but also alleviate the bipolar thermal conductivity, all of which result in the increased peak value of *ZT*. The maximum *ZT* value of ~ 0.8 is obtained at 873 K when $x = 0.06$.

Luo *et al.* investigated the thermoelectric properties of the $AgSn_mSbSe_{m+2}$ system with $m = 1$–20.[119] When $m = 1$ (i.e., $AgSnSbSe_3$), the alloy forms a stable cation-disordered cubic rock-salt structure. $AgSnSbSe_3$ has a low lattice thermal conductivity of ~ 0.47 $W{\cdot}m^{-1}{\cdot}K^{-1}$ at 673 K. The authors further added the Te element. The alloying on Se sites results in a NaCl-type solid solution $AgSnSbSe_{3-x}Te_x$ (x is in the range of 0–3) with randomly disordered cations and anions. As shown in Fig. 8(a), ΔS (the difference between the actual and ideal entropies of mixing) increases with x, arrives at the peak value of 17.3 $J{\cdot}mol^{-1}{\cdot}K^{-1}$ at $x = 1.5$, and then decreases. In Fig. 8(b), the thermal conductivity changes with x following a U-shaped curve. This U-shaped dependence occurs at all the studied temperatures, demonstrating obvious component dependent lattice thermal conductivity. At 673 K, a glass-like lattice thermal conductivity of ~ 0.32 $W{\cdot}m^{-1}{\cdot}K^{-1}$ is obtained when $x = 1.5$, indicating the feasibility of entropy engineering in decreasing lattice thermal conductivity. Figure 8(c) provides a deep understanding of such low lattice thermal conductivity. In HEAs, the increase in configurational entropy would enhance the phonon scattering strength (Γ_{total}), contributing to the phonon scattering processes due to atomic mass fluctuation (Γ_{M}) and strain field fluctuation (Γ_{S}). As shown in Fig. 8(c), all the calculated phonon scattering rates show an inverted U-shaped dependence on the x value (Te composition). Furthermore, the strain field fluctuations dominate the phonon scattering in the $AgSnSbSe_{3-x}Te_x$ HEAs. Therefore, such low thermal conductivity in $AgSnSbSe_{1.5}Te_{1.5}$ is a result of the high-entropy engineering. In addition to the impact on lattice thermal conductivity, the Te alloying also results in greater convergence of the multiple valence band maximum, and promotes a high-power factor. For $AgSnSbSe_{1.5}Te_{1.5}$, a high average power factor of ~ 9.54 $\mu W{\cdot}cm^{-1}{\cdot}K^{-2}$ and a high average *ZT* of ~ 1.0 are achieved in the range of 400 K–773 K. For $AgSnSbSe_{1.5}Te_{1.5}$, in this temperature range, a peak thermoelectric *ZT* of 1.14 is observed at 723 K, as shown in Fig. 8(d).

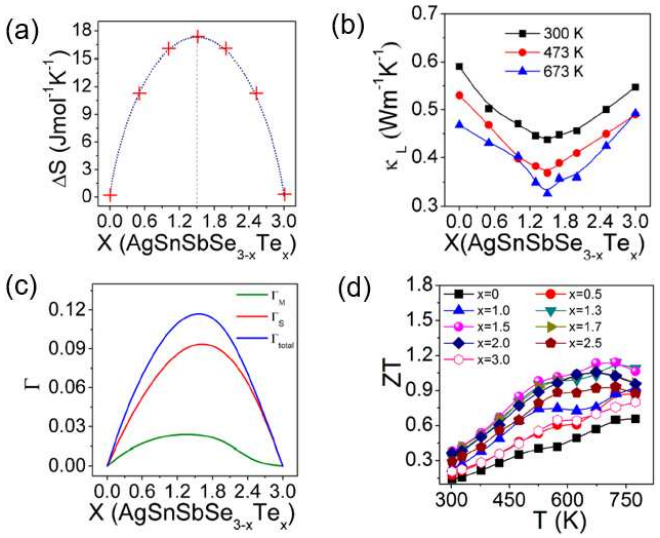


Fig. 8. (a) Calculated configurational entropy ΔS for $AgSnSbSe_{3-x}Te_x$. (b) Lattice thermal conductivity for $AgSnSbSe_{3-x}Te_x$ samples. (c) Phonon scattering parameters as a function of Te content. Here Γ_{total}, Γ_{M}, and Γ_{S} are the total scattering rate, and phonon scattering rates induced by mass fluctuation and strain field fluctuation, respectively. (d) Temperature-dependent *ZT* values for $AgSnSbSe_{3-x}Te_x$ samples.[119] For more details, please refer to Ref. [119].

Hu *et al.* investigated the thermoelectric properties of multi-principal-element-alloyed SnTe (Sn/Te/Ge/Pb/Mn alloys) both theoretically and experimentally.[120] It was found that both the absolute value of the Seebeck coefficient and carrier mobility can increase with the number of alloying elements, due to the band convergence effect.[121] Meanwhile, ultralow lattice thermal conductivity of about 0.32 $W{\cdot}m^{-1}{\cdot}K^{-1}$ at 900 K was reported in $(Sn_{0.7}Ge_{0.2}Pb_{0.1})_{0.75}Mn_{0.275}Te$ alloy, which is lower than the amorphous limit of SnTe. Combined with the increased Seebeck coefficient and electrical conductance, fine tuning of the Sn can lead to a state-of-the-art value of $ZT \approx 1.42$ at 900 K in $(Sn_{0.74}Ge_{0.2}Pb_{0.1})_{0.75}Mn_{0.275}Te$. However, if the entropy of mixing is too high, the increased mass and strain fluctuations may suppress carrier mobility, thus precise entropy engineering is required.

Tin telluride (SnTe) is another representative group-IV metal chalcogenide compound with promising thermoelectric properties. HEAs form based on PbTe, GeTe, and MnTe coalloyed with SnTe have been synthesized and studied experimentally.[122] Because of the inclusion of various elements at the cationic (Sn, Pb, Ge, and Mn) site, the configurational entropy increases, and the lattice thermal conductivity is significantly suppressed to 0.6 $W{\cdot}m^{-1}{\cdot}K^{-1}$ at room temperature. With Ga doping to optimize the carrier concentration to $\sim 5.7 \times 10^{20}$ cm^{-3}, a peak value of $ZT \sim 1.52$ is achieved at 823 K, and a high average *ZT* value ~ 1.0 in the range of 323 K–823 K is obtained in $Ga_{0.025}(Sn_{0.25}Pb_{0.25}Mn_{0.25}Ge_{0.25})_{0.975}Te$.

Importantly, except above entropy engineering to enhance the thermoelectric performance by tuning the lattice thermal conductivity and Seebeck coefficient, the phase formation, electronic band structure, and multiatomic bonding also play important roles in promoting thermoelectric performance. For example, an ultra-high thermoelectric figure of merit of about 2.0 can be obtained, when the Bi_2Te_3 systems transfer from a topologically trivial into a non-trivial phase, while the thermoelectric figure of merit also suggests a dependence on the thickness.[123] The bandgap of the PbTe–SrTe alloy can be improved by the substitution of Mn for Pb atoms. Besides, the average thermoelectric figure of Mn-doped PbTe alloy merit can be enhanced by 18%, which results from the synergistic effects of the dislocation scattering on phonon transport and band structure.[53] $Fe_2V_{0.8}W_{0.2}Al$ thin film presents a high intrinsic figure of merit, which is contributed by a Weyl-like electron dispersion near the Fermi level and the significant charge density difference at the Fermi level. Thus, a high mobility of carriers is obtained by linear crossing in the electronic bands.[55] As for the multiatomic bonding, the Bi atoms in $YbMnBi_2$ can be divided into two types, one bonded with Mn, while another shows an interlayer in-between. Such heavy Bi atom possesses an obvious spin orbital coupling effect, while the electronic bands are very light near the Fermi level, induced by the hybridisation of p and d orbitals. Therefore, high mobility and low resistivity are addressed and the decent thermoelectric figure of merit can be obtained.[124]

3.4. Developing high thermoelectric performance

Although considerable investigations have been explored to explore the thermoelectric performance of HEAs, optimizing the thermoelectric property of HEAs is an urgent issue that requires attention. Nanostructures in bulk thermoelectrics show effective phonon scattering, while the phonons possessing long mean free paths maintain unaffected. Based on this, scattering the phonons with long mean free paths to suppress the lattice thermal conductivity, so that the thermoelectric performance can be improved in experiment,[125] is an efficient strategy. Doping is a popular means to tune the properties of the materials, which also can improve the *ZT*. For example, the incorporation of the Ag and Se atoms combined with the employing entropy optimization can decrease the thermal conductivity significantly because of the anharmonicity, while the electrical conductivity is retained.[126] Thus, the outstanding power factor is obtained.

Topological thermoelectrics provide a theoretical guidance for the design of high thermoelectric performance HEAs. Even if topological insulators are promising candidates for excellent thermoelectric materials possessing intrinsic characteristics with a small bandgap and heavy element, such as Bi_2Se_3,[127–129] metals also can act as potential thermoelectrics. For example, the $YbMnSb_2$ suggests a high Seebeck coefficient and power factor comparing with other topological materials, because the obvious dispersion of the Dirac bands reduces the resistivity.[130] Therefore, the excellent thermoelectric performance together with gap free cross bands and regular bands in new topology HEAs is quite promising,[131] and combining the further application of other technologies, potential thermoelectric enhancement in HEAs can be expected.

4. Conclusion and prospects

The up-to-date investigations of the HEAs have proposed various outstanding performances, which enable potential wide applications of HEAs in thermoelectric energy conversion. This work presents a comprehensive review of the definition and the inherent superior performance of the HEAs. The structural particularity of the HEAs is addressed by definition, including crystalline, quasicrystalline and amorphous performances. The advanced applications as thermoelectric materials using HEAs are further demonstrated by explaining the novel properties of phonons.

Although remarkable advancements in the experimental and theoretical understanding of the thermoelectric properties of HEAs have been achieved, because of the complexity of HEAs, further investigations combining experimental and theoretical efforts are still indispensable. Firstly, the calculation of the phase diagram functional is a commonly used method for HEA design by calculating the equilibrium phases, but it has a strong dependence on the database, which also restricts the accuracy.[132] Thus, the development of multicomponent systems is necessary. Extensive progress has been explored considering the application of machine learning methods in computational materials science. Machine learning and high-throughput computation methods play essential roles in the field of thermoelectric materials based on HEAs. On the other side, the first principle simulations can provide the physical parameters for the calculation of phase diagrams,[133] which possesses intrinsic advantages and more advanced challenges for the prediction of HEAs.

Furthermore, to realize the actual applications of HEA-based thermoelectric devices, some crucial issues should be addressed. First, it is critical to explore an economical, efficient and high-quality production method for the HEAs, which is still a challenging topic. Second, the operability of the precise doping and functionalization is still challenging in HEAs, although it is a commonly used strategy to enhance the value of *ZT*. Moreover, the electronic conductivity and Seebeck coefficient of the current HEAs need to be further enhanced, which could be achieved by searching for proper dopants to induce band convergence. In conclusion, we believe that the thermoelectric property of HEAs is an active research topic, and continuous theoretical and experimental studies deserve to

understand the underlying physical insights, as well as boost further advancement towards the practical application.

Acknowledgment

Project supported by the Natural Science Foundation of Jiangsu Province of China (Grant Nos. BK20220407 and BK20220428).

References

[1] Baddoo N 2008 *J. Constr. Steel Res.* **64** 1199
[2] Jr Starke E A and Staley J T 1996 *Prog. Aerosp. Sci.* **32** 131
[3] Ezugwu E, Wang Z and Machado A 1999 *J. Mater. Process. Technol.* **86** 1
[4] Gray J and Luan B 2002 *J. Alloys Compd.* **336** 88
[5] Wu Z and Curtin W A 2015 *Nature* **526** 62
[6] Bellouard Y 2008 *Mater. Sci. Eng. A* **481** 582
[7] Wang D Y, Wei C Y, Lin M C, Pan C J, Chou H L, Chen H A, Gong M, Wu W, Yuan C, Angell M, Hsieh Y, Chen Y, Wen C, Chen C, Hwang B, Chen C and Dai H 2017 *Nat. Commun.* **8** 14283
[8] Li X, Lu L, Li J, Zhang X and Gao H 2020 *Nat. Rev. Mater.* **5** 706
[9] Yang Y, Chen T, Tan L, Poplawsky J D, An K, Wang Y, Samolyuk G D, Littrell K, Lipini A R, Borisevich A and George E P 2021 *Nature* **595** 245
[10] Chen X, Wang Q, Cheng Z, Zhu M, Zhou H, Jiang P, Zhou Q, Xue Q, Yuan F, Zhu J, Wu X and Ma E 2021 *Nature* **592** 712
[11] Peng S, Wei Y and Gao H 2020 *Proc. Natl. Acad. Sci. USA* **117** 5204
[12] Hinterleitner B, Knapp I, Poneder M, Shi Y, Müller H, Eguchi G, Eisenmenger-Sittner C, Stöger-Pollach M, Kakefuda Y, Kawamoto N, Guo Q, Baba T, Mori T, Ullah S, Chen X Q and Bauer E 2019 *Nature* **576** 85
[13] Yin B, Yoshida S, Tsuji N and Curtin W A 2020 *Nat. Commun.* **11** 2507
[14] George E P, Raabe D and Ritchie R O 2019 *Nat. Rev. Mater.* **4** 515
[15] Al Zoubi W, Putri R A K, Abukhadra M R and Ko Y G 2023 *Nano Energy* **110** 108362
[16] Liu X, Zhang J and Pei Z 2023 *Prog. Mater. Sci.* **131** 101018
[17] Cantor B, Chang I T H, Knight P and Vincent A J B 2004 *Mater. Sci. Eng. A* **375** 213
[18] Yeh J W, Chen S K, Lin S J, Gan J Y, Chin T S, Shun T T, Tsau C H and Chang S Y 2004 *Adv. Eng. Mater.* **6** 299
[19] Pickering E J and Jones N G 2016 *Int. Mater. Rev.* **61** 183
[20] George E P, Curtin W A and Tasan C C 2020 *Acta Mater.* **188** 435
[21] Zhou Y J, Zhang Y, Wang Y L and Chen G L 2007 *Appl. Phys. Lett.* **90** 181904
[22] Zou Y, Ma H and Spolenak R 2015 *Nat. Commun.* **6** 7748
[23] Niu C, LaRosa C R, Miao J, Mills M J and Ghazisaeidi M 2018 *Nat. Commun.* **9** 1363
[24] Liang Y J, Wang L, Wen Y, Cheng B, Wu Q, Cao T Q, Xiao Q, Xue Y F, Sha G, Wang Y D, Ren Y, Li X Y, Wang L, Wang F C and Cai H N 2018 *Nat. Commun.* **9** 4063
[25] Ding Q, Zhang Y, Chen X, Fu X, Chen D, Chen S J, Gu L, Wei F, Bei H B, Gao Y F, Wen M R, Li J X, Zhang Z, Zhu T, Ritchie R O and Yu Q 2019 *Nature* **574** 223
[26] Zou Y, Wheeler J M, Ma H, Okle P and Spolenak R 2017 *Nano Lett.* **17** 1569
[27] Ren K, Chen J, Wang H and Huang Z 2021 *J. Phys. Conf. Ser.* **2044** 012051
[28] Li Q, Zhang T W, Qiao J W, Ma S G, Zhao D, Lu P and Wang Z H 2020 *J. Alloys Compd.* 816
[29] Li D, Li C, Feng T, Zhang Y, Sha G, Lewandowski J J, Liaw P R and Zhang Y 2017 *Acta Mater.* **123** 285
[30] Wang S, Wu M, Shu D, Zhu G, Wang D and Sun B 2020 *Acta Mater.* **201** 517
[31] Hemphill M A, Yuan T, Wang G Y, Yeh J W, Tsai C W, Chuang A and Liaw P K 2012 *Acta Mater.* **60** 5723
[32] Wu J M, Lin S J, Yeh J W, Chen S K, Huang Y S and Chen H C 2006 *Wear* **261** 513
[33] Liu C, Peng W, Jiang C S, Guo H, Tao J, Deng X and Chen Z 2019 *J. Mater. Sci. Technol.* **35** 1175
[34] Chang X, Zeng M, Liu K and Fu L 2020 *Adv. Mater.* **32** 1907226
[35] Tang Y, Wang R, Xiao B, Zhang Z, Li S, Qiao J, Bai S, Zhang Y and Liaw P K 2023 *Prog. Mater. Sci.* **135** 101090
[36] Tsai M H 2013 *Entropy* **15** 5338
[37] Borkar T, Chaudhary V, Gwalani B, Choudhuri D, Mikler C V, Soni V, Aalm T, Ramanujan R V and Banerjee R 2017 *Adv. Eng. Mater.* **19** 1700048
[38] Lucas M S, Mauger L, Muñoz J A, Xiao Y, Sheets A O, Semiatin S L, Horwath J and Turgut Z 2011 *J. Appl. Phys.* **109** 07E307
[39] Kao Y, Chen S, Chen T, Chu P, Yeh J and Lin S 2011 *J. Alloys Compd.* **509** 1607
[40] Zhang Y, Xu P, Zhu J, Yan S, Zhang J and Li L 2023 *Mater. Today Phys.* **32** 101031
[41] Braic V, Balaceanu M, Braic M, Vladescu A, Panseri S and Russo A 2012 *J. Mech. Behav. Biomed. Mater.* **10** 197
[42] Kong K, Hyun J, Kim Y, Kim W and Kim D 2019 *J. Power Sources* **437** 226927
[43] Yan X and Zhang Y 2020 *Scr. Mater.* **187** 188
[44] Cheng Y, Wu X, Zhang Z, Sun Y, Zhao Y, Zhang Y and Zhang G 2021 *Nanoscale* **13** 1425
[45] Ren K, Wang K, Cheng Y, Tang W and Zhang G 2020 *Nano Futures* **4** 032006
[46] Chang J, Wang G, Li C, He Y, Zhu Y, Zhang W, Sajid M, Kara A, Gu M and Yang Y 2023 *Joule* **7** 587
[47] Zhang D, Shi Y, Zhao H, Qi W, Chen X, Zhan T, Li S, Yang B, Sun M, Lai J, Huang B and Wang L 2021 *J. Mater. Chem. A* **9** 889
[48] Li H, Han Y, Zhao H, Qi W, Zhang D, Yu Y, Cai W, Li S, Lai J, Huang B and Wang L 2020 *Nat. Commun.* **11** 5437
[49] Chen Z J, Zhang T, Gao X Y, Huang Y J, Qin X H, Wang Y F, Zhao K, Peng X, Zhang C, Liu L, Zeng M and Yu H 2021 *Adv. Mater.* **33** 2101845
[50] Jin Z, Lv J, Jia H, Liu W, Li H, Chen Z, Lin X, Xie G, Liu X, Sun S and Qiu H J 2019 *Small* **15** 1904180
[51] Zhang G and Li B 2010 *Nanoscale* **2** 1058
[52] Zhang G and Zhang Y 2017 *J. Mater. Chem. C* **5** 7684
[53] Luo J, You L, Zhang J, Guo K, Zhu H, Gu L, Yang Z, Li X, Yang J and Zhang W 2017 *ACS Appl. Mater. Interfaces* **9** 8729
[54] Xie W, Tang X, Yan Y, Zhang Q and Tritt T M 2009 *J. Appl. Phys.* **105** 113713
[55] Hinterleitner B, Knapp I, Poneder M, Shi Y, Müller H, Eguchi G, Eisenmenger-Sittner C, Stöger-Pollach M, Kakefuda Y, Kawamoto N, Guo Q, Baba T, Mori T, Ullah S, Chen X and Bauer E 2019 *Nature* **576** 85
[56] Cantor B, Chang I T H, Knight P and Vincent A J B 2004 *Mater. Sci. Eng. A* **375** 213
[57] Yeh J, Chen S, Lin S, Gan J, Chin T, Shun T, Tsau C and Chang S 2004 *Adv. Eng. Mater.* **6** 299
[58] Zhang Y, Zuo T, Tang Z, Gao M C, Dahmen K A, Liaw P K and Lu Z P 2013 *Prog. Mater. Sci.* **61** 1
[59] Yeh J 2013 *J. Met.* **65** 1759
[60] Li Z, Zhao S, Ritchie R O and Meyers M A 2019 *Prog. Mater. Sci.* **102** 296
[61] Cantor B 2021 *Prog. Mater. Sci.* **120** 100754
[62] Li W, Xie D, Li D, Zhang Y, Gao Y and Liaw P K 2021 *Prog. Mater. Sci.* **118** 100777
[63] Zhang Y, Zhou Y, Lin J, Chen G and Liaw P K 2008 *Adv. Eng. Mater.* **10** 534
[64] Senkov O N, Wilks G B, Scott J M and Miracle D B 2011 *Intermetallics* **19** 698
[65] Huo W, Fang F, Zhou H, Xie Z, Shang J and Jiang J 2017 *Scr. Mater.* **141** 125
[66] Li Z, Pradeep K G, Deng Y, Raabe D and Tasan C C 2016 *Nature* **534** 227
[67] Wang X, Guo W and Fu Y 2021 *J. Mater. Chem. A* **9** 663
[68] Tsai K Y T M and Yeh J W 2013 *Acta Mater.* **61** 4887
[69] Tsai M, Yeh J and Gan J 2008 *Thin Solid Films* **516** 5527
[70] Huo W, Wang S, Zhu W, Zhang Z, Fang F, Xie Z and Jiang J 2021 *Tungsten* **3** 161
[71] Tsai M 2013 *Entropy* **15** 5338
[72] Huo W, Liu X, Tan S, Fang F, Xie Z, Wang S and Jiang J 2021 *Appl. Surf. Sci.* **439** 222
[73] Ranganathan S 2003 *Curr. Sci.* **85** 1404

[74] Ding Q, Zhang Y, Chen X, Fu X, Chen D, Chen S, Gu L, Wei F, Bei H, Gao Y, Wen M, Li J, Zhang Z, Zhu T, Ritchie R and Yu Q 2019 *Nature* **574** 223

[75] Yeh J 2006 *Ann. Chim. Sci. Mater.* **31** 633

[76] Gludovatz B, Hohenwarter A, Catoor D, Chang E H, George E P and Ritchie R O 2014 *Science* **345** 1153

[77] Takeuchi A, Amiya K, Wada T, Yubuta K and Zhang W 2014 *J. Met.* **66** 1984

[78] Wang L, Zhang F, Nie Z, Wang L, Wang F, Wang B, Zhou S, Xue Y, Cheng B, Lou H, Chen X, Ren Y, Brown D E, Prakapenka V, Greenberg E, Zeng Z and Zeng Q 2019 *Mater. Today Phys.* **8** 1

[79] Otto F, Yang Y, Bei H and George E P 2013 *Acta Mater.* **61** 2628

[80] Liang Y, Wang L, Wen Y, Cheng B, Wu Q, Cao T, Xiao Q, Xue Y, Sha G, Wang Y, Ren Y, Li X, Wang L, Wng F and Cai H 2018 *Nat. Commun.* **9** 4063

[81] Jiang S H, Wang H, Wu Y, Liu X J, Chen H H, Yao M J, Gault B, Ponge D, Raabe D, Hirata A, Chen M W, Wang Y D and Lu Z P 2017 *Nature* **544** 460

[82] Xie C X, Li W, Zheng D H, Wang K W, Yang Y Z, Shen F H, Xie L, Liao Z L and Zhong S Y 2019 *J. Non-Cryst. Solids* **514** 20

[83] Huo J T, Huo L S, Men H, Wang X M, Inoue A, Wang J Q, Chang C T and Li R W 2015 *Intermetallics* **58** 31

[84] Li C Z, Li Q, Li M C, Chang C T, Li H X, Dong Y Q and Sun Y F 2019 *J. Alloys Compd.* **791** 947

[85] Wu W, Ni S, Liu Y, Liu B and Song M 2017 *Mater. Charact.* **127** 111

[86] Li R, Gao J C and Fan K 2011 *Mater. Sci. Forum* **686** 235

[87] Takeuchi A, Amiya K and Yubuta K 2018 *Mater. Chem. Phys.* **210** 245

[88] Mao J, Chen G and Ren Z 2021 *Nat. Mater.* **20** 454

[89] Zhang G, Zhang Q, Bui C, Lo G and Li B 2009 *Appl. Phys. Lett.* **94** 213108

[90] Chen K, Li W, Duan W, Shuai Z and Gu B 2005 *Phys. Rev. B* **72** 045422

[91] Hu L, Zhu T, Liu X and Zhao X 2014 *Adv. Funct. Mater.* **24** 5211

[92] Ouyang Y, Zhang Z, Li D, Chen J and Zhang G 2019 *Ann. Phys.* **531** 1800437

[93] Zhang G and Zhang Y 2013 *Phys. Status Solidi* **7** 754

[94] Jiang B, Yu Y, Cui J, Liu X, Xie L, Liao J, Zhang Q, Huang Y, Ning S and Jia B 2021 *Science* **371** 830

[95] Jiang B, Wang W, Liu S, Wang Y, Wang C, Chen Y, Xie L, Huang M and He J 2022 *Science* **377** 208

[96] Xie G, Shen Y, Wei X, Yang L, Xiao H, Zhong J and Zhang G 2014 *Sci. Rep.* **4** 5058

[97] Liu R, Chen H, Zhao K, Qin Y, Jiang B, Zhang T, Sha G, Shi X, Uher C and Zhang W 2017 *Adv. Mater.* **29** 1702712

[98] Yang J, Meisner G and Chen L 2004 *Appl. Phys. Lett.* **85** 1140

[99] Meisner G, Morelli D, Hu S, Yang J and Uher C 1998 *Phys. Rev. Lett.* **80** 3551

[100] Plirdpring T, Kurosaki K, Kosuga A, Day T, Firdosy S, Ravi V, Snyder G J, Harnwunggmoung A, Sugahara T and Ohishi Y 2012 *Adv. Mater.* **24** 3622

[101] Sun M, Chou J, Shi L, Gao J, Hu A, Tang W and Zhang G 2018 *ACS Omega* **3** 5971

[102] Wei P C, Liao C N, Wu H J, Yang D, He J, Biesold-McGee G V, Liang S, Yen W T, Tang X and Yeh J W 2020 *Adv. Mater.* **32** 1906457

[103] Körmann F, Ikeda Y, Grabowski B and Sluiter M 2017 *NPJ Comput. Mater.* **3** 36

[104] Chen S and Ren Z 2013 *Mater. Today* **16** 387

[105] Shafeie S, Guo S, Hu Q, Fahlquist H, Erhart P and Palmqvist A 2015 *J. Appl. Phys.* **118** 184905

[106] Karati A, Nagini M, Ghosh S, Shabadi R, Pradeep K, Mallik R C, Murty B and Varadaraju U 2019 *Sci. Rep.* **9** 5331

[107] Karati A, Hariharan V, Ghosh S, Prasad A, Nagini M, Guruvidyathri K, Mallik R C, Shabadi R, Bichler L and Murty B 2020 *Scr. Mater.* **186** 375

[108] Shi X, Zou J and Chen Z 2020 *Chem. Rev.* **120** 7399

[109] Li J, Tan Q, Li J F, *et al.* 2013 *Adv. Funct. Mater.* **23** 4317

[110] Zheng Y, Zhang Q, Su X, Xie H, Shu S, Chen T, Tan G, Yan Y, Tang X and Uher C 2015 *Adv. Energy Mater.* **5** 1401391

[111] Yu C, Zhang G, Zhang Y and Peng L 2015 *Nano Energy* **17** 104

[112] Fan Z, Wang H, Wu Y, Liu X and Lu Z 2016 *RSC Adv.* **6** 52164

[113] Yan X, Poudel B, Ma Y, Liu W, Joshi G, Wang H, Lan Y, Wang D, Chen G and Ren Z 2010 *Nano Lett.* **10** 3373

[114] Ivanov O, Yaprintsev M, Vasil'ev A and Yaprintseva E 2021 *J. Alloys Compd.* **872** 159743

[115] Yamashita A, Goto Y, Miura A, Moriyoshi C, Kuroiwa Y and Mizuguchi Y 2021 *Mater. Res. Lett.* **9** 366

[116] Heremans J P, Jovovic V, Toberer E S, Saramat A, Kurosaki K, Charoenphakdee A, Kurosaki K, Charoenphakdee A, Yamanaka S and Snyder G J 2008 *Science* **321** 554

[117] Zhan S, Zheng L, Xiao Y and Zhao L 2020 *Chem. Mater.* **32** 10348

[118] Fan Z, Wang H, Wu Y, Liu X and Lu Z 2017 *Mater. Res. Lett.* **5** 187

[119] Luo Y, Hao S, Cai S, Slade T J, Luo Z Z, Dravid V P, Wolverton C, Yan Q and Kanatzidis M G 2020 *J. Am. Chem. Soc.* **142** 15187

[120] Hu L, Zhang Y, Wu H, Li J, Li Y, Mckenna M, He J, Liu F, Pennycook S J and Zeng X 2018 *Adv. Energy Mater.* **8** 1802116

[121] Liu W, Tan X, Yin K, Liu H, Tang X, Shi J, Zhang Q and Uher C 2012 *Phys. Rev. Lett.* **108** 166601

[122] Wang X, Yao H, Zhang Z, Li X, Chen C, Yin L, Hu K, Yan Y, Li Z and Yu B 2021 *ACS Appl. Mater. Interfaces* **13** 18638

[123] Liang J, Cheng L, Zhang J, Liu H and Zhang Z 2016 *Nanoscale* **8** 8855

[124] Pan Y, Le C, He B, Watzman S J, Yao M, Gooth J, Heremans J P, Sun Y and Felser C 2022 *Nat. Mater.* **21** 203

[125] Biswas K, He J, Blum I D, Wu C I, Hogan T P, Seidman D N, Dravid V P and Kanatzidis M G 2012 *Nature* **489** 414

[126] Ahmad A, Zhu B, Wang Z, Gui Z, Wang W, Wang T, Yu Y, Huang L and He J 2024 *Energy Environ. Sci.* **17** 695

[127] Min Y, Roh J W, Yang H, Park M, Kim S I, Hwang S, Lee S M, Lee K H and Jeong U 2013 *Adv. Mater.* **25** 1424

[128] Shahil K, Hossain M, Goyal V and Balandin A 2012 *J. Appl. Phys.* **111** 054305

[129] Alegria L, Schroer M, Chatterjee A, Poirier G, Pretko M, Patel S and Petta J 2012 *Nano Lett.* **12** 4711

[130] Pan Y, Fan F R, Hong X, He B, Le C, Schnelle W, He Y, Imasato K, Borrmann H and Hess C 2021 *Adv. Mater.* **33** 2003168

[131] Yang T, Yang Y, Wang X, Zhang G and Cheng Z 2023 *Mater. Today Chem.* **30** 101488

[132] Ma Y J, Ma Y, Wang Q, Schweidler S, Botros M, Fu T, Hahn H, Brezesinski T and Breitung B 2021 *Energy Environ. Sci.* **14** 2883

[133] Li R, Xie L, Wang W, Liaw P and Zhang Y 2020 *Front. Mater.* **7** 290